Neutron Flux Intercomparison at NBS

Kenneth C. Duvall, Michael M. Meier, and Oren A. Wasson

Center for Radiation Research, National Bureau of Standards, Washington, DC 20234

Vinh D. Huynh

Bureau Internaltional des Poids et Mesures, Sevres, France

August 8, 1978

National Bureau of Standards (NBS) participation in an International Bureau of Weights and Measures (BIPM) sponsored neutron flux intercomparison is described. The efficiencies of two transfer instruments, a gas-filled ^{3}He proportional counter and a BF$_3$ counter imbedded in a polyethylene sphere, were determined at neutron energies of 250 keV and 560 keV. The efficiency of the ^{3}He detector was determined by placing it in the flux monitored by the NBS "black" detector. Since the polyethylene sphere detector shadows the "black" detector, a secondary BF$_3$ counter was calibrated and it normalized the sphere and "black" detector runs. The efficiencies are reported and compared to the quantities determined at other participating standards laboratories.

Key words: Calibration standards; efficiency; international comparisons; neutron detectors; neutron flux.

1. Introduction

The International Bureau of Weights and Measures (BIPM) is sponsoring an intercomparison of neutron flux monitoring at the major international standards laboratories. NBS participation occurred during the period December 1 to 15, 1976 at the neutron flux facility associated with the 3 MV positive ion Van de Graaff. Flux monitoring at this facility is done with a "black" neutron detector which has been calibrated through the associated particle technique and calculated using a Monte Carlo program. The NBS flux was intercompared at neutron energies of 250 and 565 keV. For these energies the intercomparison monitors used in the program are a ^{3}He gas filled proportional counter and a BF$_3$ counter imbedded in a polyethylene sphere.

All other standards laboratories use an open geometry for measurements and the intercomparison is usually performed with the BIPM intercomparison monitor and the laboratory flux monitor symmetrically located equidistant from the neutron source. Since the NBS system employs a single beam, collimated and monitored at 0°, use of this technique was not possible. Instead, the "black" detector was used to calibrate a secondary monitor at a back angle and the latter was used to normalize intercomparison monitor and "black" detector runs.

Backgrounds for the "black" detector were measured using pulsed beam techniques. Since the transfer instruments were too slow for time-of-flight (TOF) measurements, backgrounds were determined in other ways. The sphere background was determined by studying the radial dependence of the count rate and by interposing a shadow bar between source and detector. Since the ^{3}He detector is a spectrometer, a curve fitting procedure could be used to discriminate against background.

The objective of the procedure was to measure an efficiency for each of the two intercomparison instruments at the two selected energies. Since measurements at other laboratories made use of the symmetry mentioned above, this efficiency was defined to include the detector geometry and no correction was made for air transmission between the neutron source and detector.

2. Experimental

2.1. Neutron Source

The source of neutrons was the ^{7}Li(p, n) reaction. Metallic lithium was vacuum evaporated onto a tantalum substrate that formed the end of the beam transport system. The targets were transported from the evaporator to the beamline in a helium atmosphere and care was taken to minimize their exposure to air. No evidence for oxidation of surface layers was seen in the threshold measurements. The target thickness was measured to be 17 keV by observing the yield from the target as a function of bombarding energy near threshold and by the width of the neutron peak observed in the black detector TOF spectrum. The target spot was defined by two collimators in the proton beam line which were also used in the neutron collimator alignment. The

discolored region where the beam struck the target indicated that the effective spot size was less than 4 mm. Target current and currents incident on each collimator were monitored throughout the experiment.

To reduce room scattered neutrons the source was surrounded with a massive shield of paraffin loaded with Li_2CO_3. Machined inserts of lithium loaded polyethylene defined the neutron beam. These were aligned, along with the shield, using the same transit that defined the proton beam and the neutron collimator axis. Alignment was facilitated by use of an air bearing that supported the shield and a set of four screws rigidly attached to the floor which located the air bearing.

2.2. Transfer Instruments

Signals from the sphere detector were preamplified, amplified, and supplied to a single channel analyzer (SCA) operated in the lower level mode. The logic output of the SCA was scaled. The discriminator level of the SCA was adjusted to give a selected rate when a calibrated source was positioned in a reproducible location in the sphere. This calibration procedure was employed on a daily basis to eliminate possible shifts in the bias level.

The ^3He detector used a similar amplifier-SCA arrangement, but the amplifier output was also supplied to a multichannel analyzer (MCA). Pulse height spectra were recorded and output for subsequent analysis.

The collimated neutron beam depicted in figure 1 has a half angle of $4.5°$. A line was scribed on the A1 floorplate below and parallel to the beam axis so that by using a plumb bob it was easy to locate the sphere detector on the axis to within ± 2 mm. Several measurements with the sphere
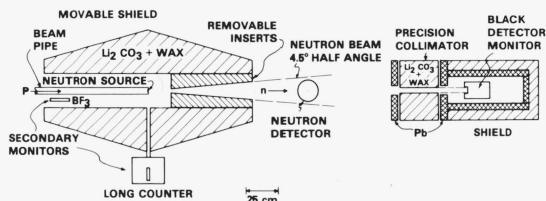

FIGURE 1. *NBS neutron flux facility.*

displaced from the axis by as much as 0.5 cm were done at a distance of 150 cm. As expected from earlier beam profile measurements, no change in response was observed. At distances closer to the target it was possible to view the target spot from behind the sphere to insure that the entire detector was in the direct flux.

The ^3He detector was displaced $2.8°$ from the neutron beam axis so that the black detector could be operated

simultaneously with no transmission correction. Earlier profile measurements indicate that the beam uniformity is such that no flux correction need be made for such a displacement. The source-detector distance was 105 cm.

2.3   Black Detector

The NE-110 black detector [1][^1] was located in a massively shielded enclosure 5.86 m from the target. A 15.5 cm^2 collimator defines the solid angle subtended by the detector and insures that all the neutron flux is incident on the reentrant hole of the detector. A transit was used to align the collimator with the neutron source. The last two proton beam collimators and the neutron collimator axis were aligned to be colinear to within 0.5 mm. The effective area of the cylindrical collimator was increased from the geometrical area to account for the divergent neutron beam. This correction was one percent.

The electronics for the black detector are shown in figure 2. The system collects data from the black detector in a 4096 channel two-parameter array; pulse height and neutron time-of-flight. The ADC's are gated by true time-of-flight events to keep dead-time associated with photomultiplier noise to a minimum.

A loss of efficiency in monitoring may occur if a neutron event is not accompanied with a stop pulse. To measure the effect, a time-to-amplitude converter (TAC) with a 2 μs
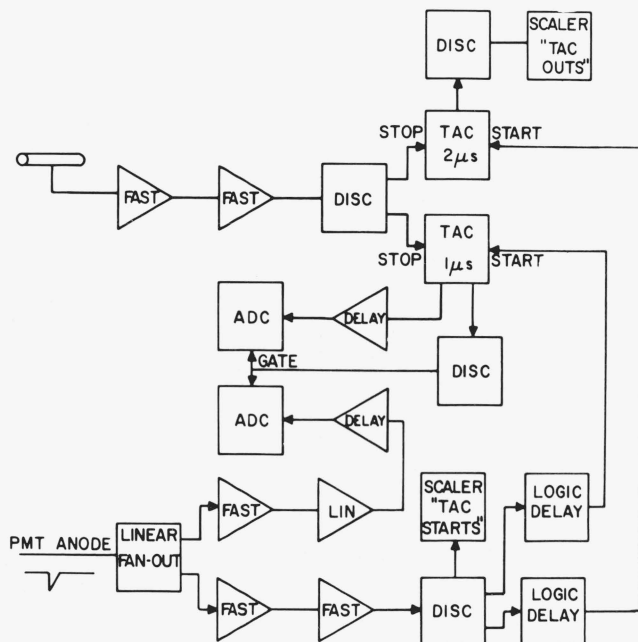

FIGURE 2. *Two-parameter data acquisition system for the black detector.*

---

[^1]: Figures in brackets indicate the literature references at the end of this paper.

range was used and valid outputs were scaled and compared to the total number of TAC starts. Discrepancies between these two numbers were always less than 0.1 percent and the data was left uncorrected for this effect. The bias was set well into the photomultiplier tube (PMT) noise for the measurement at 250 keV and it was not possible to make this check due to multiple firing of the discriminator.

The ADC's were read by a special unit [2] which converted the two outputs into a single address in a 32 (time) × 128 (pulse-height) array. This was done so that address generation could be done by hardware, rather than the relatively time-consuming software, thereby reducing dead-time. This address was acquired by the computer through CAMAC and the approprite location in memory was incremented. A separate ADC was used to record the time-of-flight spectrum in the computer. The data acquisition program was triggered at the highest available priority and dead-time was calculated and incremented in the course of each program execution.

2.4. Secondary Monitors

Since the black detector could not be used with the polyethylene sphere shadowing the beam, several secondary monitors were used to normalize sphere and black detector runs. The shield surrounding the source has a 2.54 cm diameter hole which views the target at an angle of 90°. A long counter (LC) mounted outside this hole was tested for use as a suitable secondary monitor. By steering the beam transversely across a distance of less than 4 mm at the target it was found that the rate in the LC varied ~10 percent. Also when the target was rotated by 30° to produce a new beam spot, the rate changed by as much as 25 percent. These effects were attributed to the transmission of neutrons through the tantalum substrate. These large changes made the long counter unacceptable as a monitor.

A second monitor was a plastic scintillator which was biased above tube noise and located at 180° to the proton beam and about 1.0 m from the target. This monitor exhibited sporadic behavior which may have been associated with sensitivity to gamma rays from collimating slits, shifts in the bias level and the fact that the neutron energies at 180° are 140 keV and 15 keV for 0° energies 565 keV and 250 keV respectively. This monitor was also rejected.

Finally, a BF_3 proportional counter was mounted on the beam pipe about 25 cm behind the target. Figure 3 shows the ratio of the rate of this detector to the black detector for an eighteeen hour period during the 250 keV sphere runs. The excellent stability of the BF_3 counter made it the obvious choice for a secondary monitor.

3. Data Collection

The procedure followed for determining the sphere efficiency consisted of calibrating the BF_3 counter relative to the
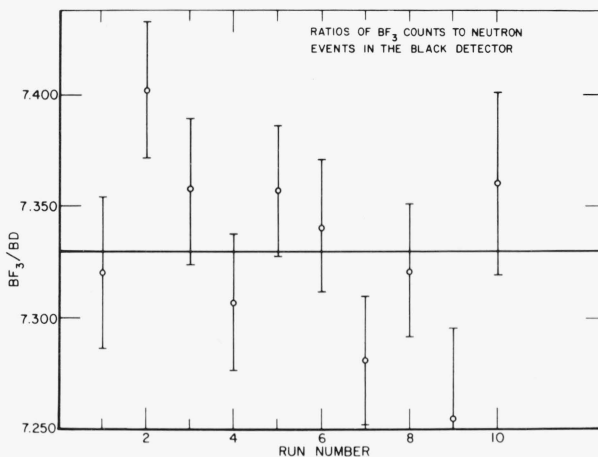

FIGURE 3. *Ratio of black detector to secondary monitor counting rates.* Error bars are based on counting statistics (1σ) for the detectors.

black detector and then taking data with the sphere detector relative to BF_3.

The ordinary sequence of runs was to alternate calibration runs with sphere runs. At frequent intervals the beamstop was used to shield the target and prevent neutron production and black detector data was taken. This provided a "beam-stop-in" background, comprised of photomultiplier noise, cosmic rays, and other events not related to neutron production at the target. For the calibration runs the two parameter pulse-height and time-of-flight spectrum as well as a single parameter time-of-flight spectrum were recorded on magnetic tape. Also recorded were computer dead-time, total integrated current, average target current, time and scaler outputs. Included in the latter were sphere events, BF_3 events, black detector starts, and black detector TAC conversions as discussed above. Sums over the pulse height spectra for each of 22 time channels in the two parameter array were also recorded. These sums permitted preliminary calculations of calibration constants as well as the influence of various background contamination. It was also possible to observe the stability of the monitors and of the pulsing system with this information.

Measurements were then made with the sphere in the beam and the above data were taken except those from the black detector since it was shadowed by the sphere. The sphere to target distance was 1.5 m for the intercomparison runs and varied between 1.4 and 3.0 m for the background determination runs. A run with a massive shadow bar interposed between source and sphere constituted a second method for background determination.

Since the ^3He counter is small it was possible to do calibration runs simultaneously with the data collection. The ^3He data were comprised of 256 channel pulse height spectra and analyzer dead-time. These were output for later analysis. The spectral sum above a given bias served for preliminary analysis.

4. Data Analysis

The count rate in the black detector is

$$R_{BD} = \varphi \, \frac{A_{\text{col}}}{(r_{\text{col}})^2} \, \epsilon \, T(r_{BD})$$

where

R_{BD} is the background and dead-time corrected rate in the black detector

φ is the neutron source strength

A_{col} is the area of the neutron collimator

r_{col} is the target-neutron collimator distance

$T(r)$ is air transmission as a function of the distance r

r_{BD} is the target-black detector distance

ϵ is the black detector efficiency

For the rate in a transfer counter, $R_c(r)$

$$R_c(r) = \varphi \, \frac{A_{\text{eff}}}{r^2} \, E' \, T(r)$$

where

A_{eff} is the effective area of the counter

r is the target-counter distance

E' is the intrinsic efficiency of the counter

We may define an efficiency* which takes into account the geometric effects:

$$E \equiv \frac{A_{\text{eff}}}{r_c^2} E'$$

where r_c is the conventional distance at which measurements are made.

Then

$$R_c(r) = \varphi \left(\frac{r_c}{r} \right)^2 T(r) E$$

Since

$$R_m = k\varphi,$$

where R_m is a monitor rate, we can obtain

$$\frac{R_{BD}}{R_m(BD)} * \frac{R_m(c)}{R_c(r)} = \frac{A_{\text{col}}}{R_{\text{col}}^2} \frac{T(r_{BD})}{T(r)} \frac{\epsilon}{E} \left(\frac{r}{r_c} \right)^2$$

Finally

$$E = \left(\frac{R_c(r)}{R_m(c)} \right) \left(\frac{R_{BD}}{R_m(BD)} \right)^{-1} \frac{A_{\text{col}}}{r_{\text{col}}^2} \left(\frac{r}{r_c} \right)^2 T(r_{BD} - r)\epsilon$$

where $R_m(c)$ is the monitor rate with the counter in position.

---

* The efficiency, E, is referred to as the "sensitivity of the transfer instrument, ϵ_0" in ref. [4].

The corrections made to quantities in the above formula and associated uncertainties are listed in table I.

TABLE I. *Corrections and Uncertainties*

Correction	Magnitude	Uncertainty
Black detector summation integral ambiguity	—	0.4%
BF$_3$ background	<0.01%	<0.01
Sphere background	1.0	1.0
Sphere deadtime	<0.01	<0.01
^{3}He uncertainty	—	0.5
Target collimator distance	—	0.07
Target counter distance	—	0.4
Air transmission	—	0.4
Black detector efficiency	—	2.5

250 keV

Correction	Magnitude	Uncertainty
Collimator area	2.8%	0.5%
Black detector background	9.0	0.8
Black detector gamma ray contamination of neutrons	1.0	0.5
Black detector deadtime	0.8	<0.01
Black detector counting statistics (1σ)	—	0.2 (Sphere)
	—	0.1 (^{3}He)
BF$_3$ counting statistics (1σ)	—	0.14 (Sphere)
	—	0.07 (^{3}He)
Sphere counting statistics (1σ)	—	0.8
^{3}He counting statistics (1σ)	—	0.8

560 keV

Correction	Magnitude	Uncertainty
Collimator area	1.6%	0.5%
Black detector background	4.0	0.4
Black detector deadtime	2.0	<0.01
Black detector counting statistics (1σ)	—	0.3 (Sphere)
	—	0.1 (^{3}He)
Bf$_3$ counting statistics (1σ)	—	0.2 (Sphere)
	—	0.1 (^{3}He)
Sphere counting statistics (1σ)	—	0.6
^{3}He counting statistics (1σ)	—	1.0

The monitor rate from the BF$_3$ counter and counter rate from the sphere were taken from the scalers associated with each and corrected for background measured with the beamstop in. Since the BF$_3$ counter served as a monitor, the ∼0.1 percent dead-time correction cancels in first order and was therefore ignored. The rate in the ^{3}He counter was obtained by summing the counts above a given pulse height level. This level was taken to be 0.6 of the pulse height difference between the thermal and fast neutron peak. This analysis was done with a fitting program designed and written for the intercomparison at BIPM [3]. The cylindrical collimator area was calculated from its measured diameter and corrected for transmission due to the beam divergence. Collimator, detector, and black detector distances were all measured with commercial scales. Transmissions through air were calculated using distances measured as above and total cross

sections from ENDF-B [4] files. Cross sections were assigned an uncertainty of 4 percent to account for a combination of inherent cross section uncertainty and possible energy shifts.

A typical black detector time-of-flight spectrum for 250 keV is schematically shown in figure 4. Time regions corresponding to neutrons (A), background (B), and gamma rays (C) are labeled. The time channels in each region were
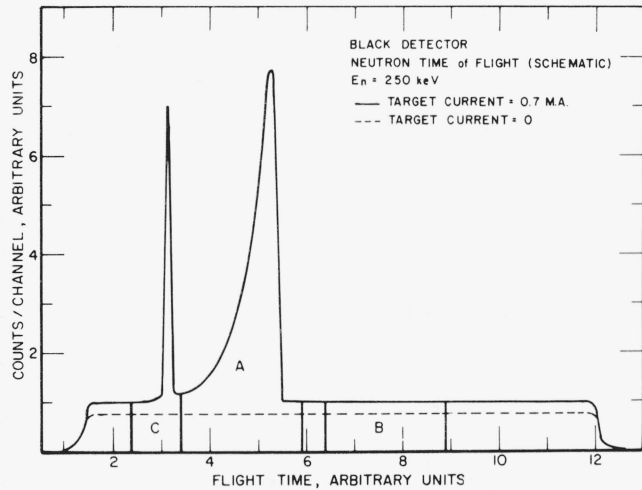

FIGURE 4. *Time-of-flight spectrum for 250 keV neutrons.*

summed to produce pulse height spectra. The same operation was done for the two parameter spectrum taken with beam-stop in to produce pulse height spectra for background. The latter was normalized and subtracted from the calibration spectrum and were found to account for roughly 80 percent of the background in region B. The remaining 20 percent background was due to neutron and gamma ray production in the target and showed no apparent structure in the reduced time spectrum. It was appropriately normalized and sub-tracted from the A and C spectra. A typical reduced C spectrum is shown in figure 5. The object of this part of the analysis was to determine the number of neutrons which were in the gamma ray time region. Since the gamma rays have relatively large light output, it was assumed that their pulse height distribution would be relatively flat in the vicinity of the 250 keV neutrons. This seems to be born out by the experimental spectrum and therefore a straight line with zero slope is fit to the high pulse height events and extrapolated to zero. The remaining events above the gamma ray were then summed and subsequently used to correct the data. It was possible to repeat the analysis, expanding the C region to successively shorter times and finding a limiting value for this correction.
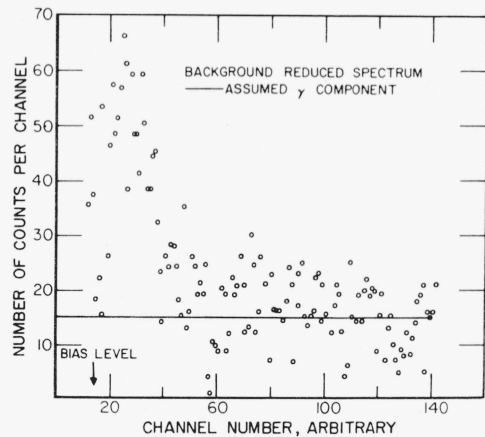

FIGURE 5. *Pulse height spectrum for the time region of gamma rays.*

Uncertainty in the background was obtained by ignoring the beam off background and making a direct subtraction of the B region from A. Changing the summation limits from 5 to 10 time channels for each region was also helpful in assessing this uncertainty.

The channel width of the reduced A spectrum was then changed to give a spectrum which could be compared with the output of CARLY, [5] the Monte Carlo program for efficiency calculation of the black detector. Usually less than three iterations of channel width changes were sufficient to produce a qualitatively good fit. Figure 6 shows a reduced spectrum at 250 keV and the corresponding CARLY calcu-lation. The value for the rate in the black detector is taken to
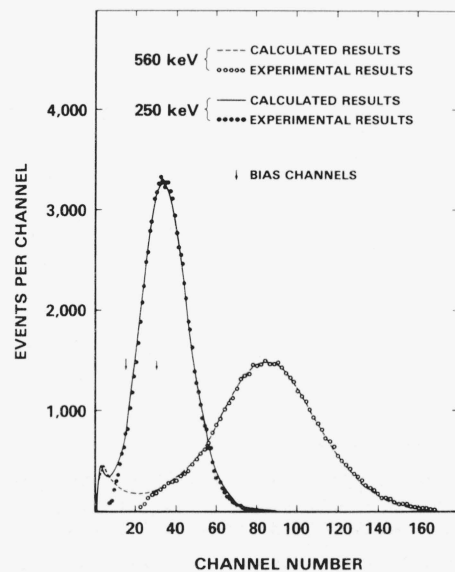

FIGURE 6. *Experimental and Monte Carlo calculated pulse height spectra.*

be the sum of counts above the indicated bias level. The corresponding efficiency is deduced from the CARLY calculation using the same bias level. It was found that the quality of the fit deteriorated appreciably when the bin width parameter was adjusted away from optimum by an amount that shifted the peak by one channel. This criterion was used in assigning an uncertainty due to bias channel ambiguity between experiment and calculation.

A schematic representation of the time-of-flight spectrum for 560 keV neutrons is shown in figure 7. Gamma rays do not complicate the analysis in this case, but additional neutrons, due to incompletely suppressed retrace pulses, appear in region C. The analysis proceeded as above except that neutrons from region C were included as part of the main peak sum. A reduced spectrum and CARLY calculation are also shown in figure 6. Finally, computer data were corrected for dead-time, and efficiencies were calculated from the above formula.
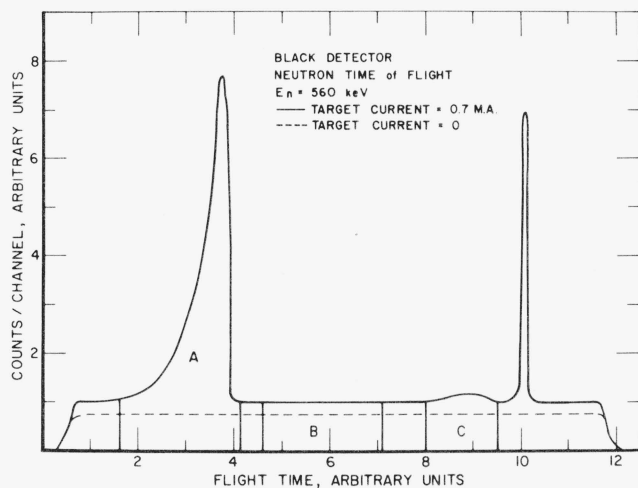
TABLE II. *Efficiency (cts/n-sr^{-1})*

E_n	Net Statistical Uncertainty	Net Systematic Uncertainty Sphere	Efficiency
250 keV	0.8%	3.0%	$4.76 \pm 0.15 \times 10^{-6}$
565 keV	0.7	2.9	$5.97 \pm 0.18 \times 10^{-6}$
		^3He	
250 keV	0.8%	2.9%	$3.20 \pm 0.09 \times 10^{-6}$
565 keV	1.0	2.7	$2.21 \pm 0.06 \times 10^{-6}$

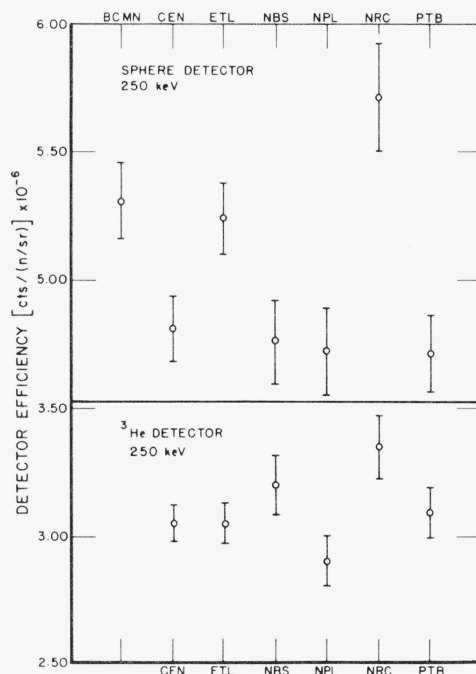FIGURE 7. *Time-of-flight spectrum for 560 keV neutrons.*

FIGURE 8. *Detector efficiency determined at 250 keV by NBS and other standards laboratories.*

BCMN— Bureau Central des Mesures Nucleaires, Geel, Belgium; CEN = Centre d'Etudes Nucleaires, Cadarache, France; ETL = Electrotechnical Laboratory, Tokyo, Japan; NBS = National Bureau of Standards, Washington, DC, U.S.A.; NPL = National Physical Laboratory, Teddington, Great Britain; NRC = National Research Council, Ottawa, Canada; PTB = Physikalisch-Technische Bundesanstalt, Braunschweig, Germany.

5.   Results

The efficiency determination of sphere and ^{3}He counters is summarized in table II. The uncertainty associated with the measurement is derived from table I by adding all applicable uncertainties in quadrature.

The 250 keV results are graphically depicted in figure 8 along with the results obtained by other standards laboratories [3]. The ^{3}He results are in fairly good agreement as are the results for both detectors at 560 keV as discussed in reference [3]. It is interesting to note that the discrepancies between laboratories for the sphere calibration are correlated with the background levels at each laboratory. The four

laboratories with the sphere efficiency of ~4.70 also reported the lowest backgrounds. These effects are much less pronounced for the ^{3}He detector which has some background discrimination and for the 560 keV energy where the ^{7}Li(p, n) source reaction is five times as prolific and the signal to background ratio is proportionately improved.

A second part of the measurement was an attempt to measure sphere background by varying the source-sphere distance. If one assumes an isotropic background resulting

from wall return and air scatter, then the neutron distribution should be of the form

$$N(r) = \frac{A}{r^2} + B,$$

where r is the source-sphere distance. The apparent efficiency of the detector will then increase as r increases and the magnitude of the background can be inferred from the magnitude of this effect. Figure 9 is a plot of the efficiency values obtained for this radial variation. It is clear that systematic uncertainties shift the data beyond the limits expected from the statistical error bars. However, no systematic rise with increasing r is observed and the contribution

of an isotropic background is less than three or four percent at 1.5 m. Another run with a massive shield designed to shadow the sphere showed no significant background above room background.

Neither result is unexpected. A shadow bar measurement is normally used to determine isotropic backgrounds in an open geometry. For the shielded geometry employed at NBS the shadow bar measurement could as well have been considered a "plugged" source run. Varying the distance, r, from source to detector is also conventionally applied to open geometry. For a shielded source the background would be expected *not* to be isotropic, but rather to originate in the components of the shield. This is a strong argument for using pulsed beam techniques and fast transfer instruments in future intercomparisons.
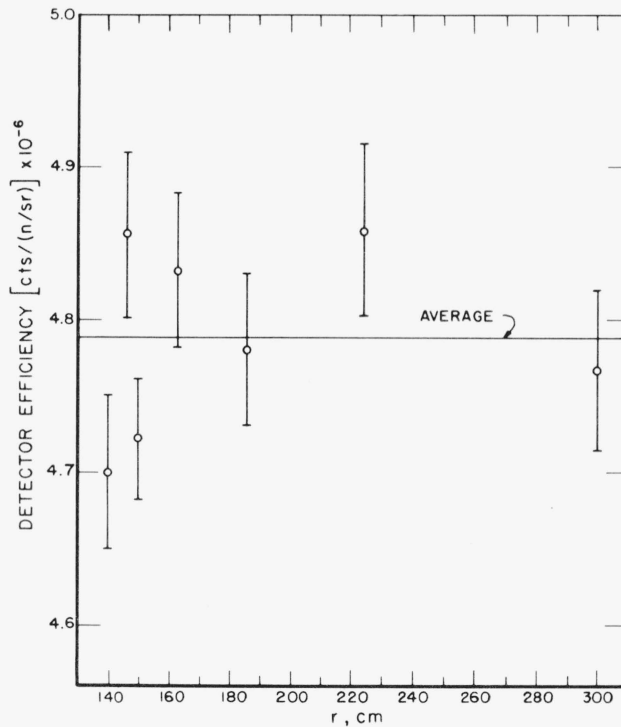

FIGURE 9. *Sphere efficiency as a function of distance from the source.*
No departure from r^{-2} behavior is evident.

6. References

[1] Lamaze, G. P., Meier, M. M., and Wasson, O. A., Conf. on Nuclear Cross Sections and Technology, Nat. Bur. Stand. (U.S.), Spec. Publ. 425, Vol. 1, pp. 73–74 (Oct. 1975).

[2] Green, David, Private communication.

[3] Huynh, V. D., International Specialists' Symp. on Neutron Standards and Applications, Nat. Bur. Stand. (U.S.), Spec. Publ. 493, p. 244, (Oct. 1977).

[4] Evaluated Nuclear Data File, Format B, Version IV, National Nuclear Data Center, Brookhaven National Laboratory, Upton, N.Y.

[5] M. M. Meier, Private communication.